


Future 3D Additive Manufacturing
The 3DMM20 Conference



**3D Nano- and
Micro-Manufacturing:
Technology and
Technical Application**

**REGISTER
NOW!**

April 3 – 8, 2022 | Schöntal Monastery, Germany

Plasmonic Properties of Colloidal Assemblies

Christian Rossner,* Tobias A. F. König,* and Andreas Fery*

The assembly of metal nanoparticles into supracolloidal structures unlocks optical features, which can go beyond synergistic combinations of the properties of their primary building units. This is due to inter-particle plasmonic coupling effects, which give rise to emergent properties. The motivation for this progress report is twofold: First, it is described how simulation approaches can be used to predict and understand the optical properties of supracolloidal metal clusters. These simulations may form the basis for the rational design of plasmonic assembly architectures, based on the desired functional cluster properties, and they may also spark novel material designs. Second, selected scalable state-of-the-art preparative strategies based on synthetic polymers to guide the supracolloidal assembly are discussed. These routes also allow for equipping the assembly structures with adaptive properties, which in turn enables (inter-)active control over the cluster optical properties.

for plasmonic NP assembly. These strategies typically involve using specific key components as linker spacer, which serve to guide the assembly process and control the supracolloidal structures: Metal oxide layers (such as silica),^[4] biomacromolecular linkers (such as DNA),^[5,6] as well as synthetic polymers are typical examples, each offering specific opportunities but also involving limitations (for a more detailed comparative discussion of these different preparative approaches, we refer to a recent review).^[7] For example, metal oxide layers create a rigid, permanent barrier, and while this feature can be very beneficial for particular investigations,^[4] it cannot be used for the development of soft adaptive systems. Assembly concepts based on DNA,^[5] on the other hand, arguably offer the synthesis of intricate and

highly complex plasmonic assemblies with unmatched structural precision, as well as enabling their dynamic switching,^[6] but at the same time their low-yield formation impedes the development of these systems into devices and applications. It is for these reasons, among others, that abiding effort is devoted to achieving the tailored assembly of plasmonic NPs by the aid of synthetic polymers. Recently, the assembly of plasmonic NPs into static supracolloidal clusters, and also the possibility of controlling their dynamic features,^[8] which becomes possible through adaptive polymers,^[9] have attracted attention.

In light of the above, in this progress report we review and discuss the scope and prospects of functional polymers to guide the formation of plasmonic NPs into responsive clusters. Other than in more comprehensive reviews on the polymer-guided assembly of plasmonic NPs,^[10] of inorganic NPs in general,^[11] or the assembly of inorganic NPs into a particular core-satellite type arrangement structure,^[7] we focus on the optical properties of different cluster assemblies and possibilities to engineer these ensemble properties. In the selection of systems presented, we have put a particular emphasis on the role of the polymer as an (inter-)active component that can adapt to external or internal triggers. Several distinct macromolecular designs recently enabled the dynamic tuning of (supra-)colloidal plasmonic systems in various ways. This is summarized in **Table 1**, which lists the different stimuli that are available to induce a material response together with the polymer component that mediates it. With this focus on plasmonic properties of (supra-)colloidal clusters controlled by polymers, the present progress report complements recent reviews that have highlighted systems with small (<5 nm) metal nanogaps,^[12] surface-enhanced Raman scattering (SERS) properties of plasmonic NP clusters,^[13] and plasmonic metasurfaces.^[14]


1. Introduction

Today, the controlled synthesis of metallic nanoparticles (NPs) with defined elemental composition, dimension, and shape,^[1] the experimental characterization of plasmonic properties^[2] as well as their simulation,^[3] are comparably developed. When supracolloidal assemblies form from these well-understood primary plasmonic entities, new collective properties emerge and complexity increases considerably. The potential for unlocking novel functionality and synergies between different nanoscale building blocks has sparked a variety of strategies

Dr. C. Rossner, Dr. T. A. F. König, Prof. A. Fery
Leibniz-Institut für Polymerforschung Dresden e. V.
Hohe Straße 6, Dresden 01069, Germany
E-mail: rossner@ipfdd.de; koenig@ipfdd.de; fery@ipfdd.de

Dr. C. Rossner, Dr. T. A. F. König, Prof. A. Fery
Center for Advancing Electronics Dresden (cfaed)
Technische Universität Dresden
Helmholtzstraße 18, Dresden 01069, Germany

Prof. A. Fery
Physical Chemistry of Polymeric Materials
Technische Universität Dresden
Bergstraße 66, Dresden 01069, Germany

 The ORCID identification number(s) for the author(s) of this article can be found under <https://doi.org/10.1002/adom.202001869>.

© 2021 The Authors. Advanced Optical Materials published by Wiley-VCH GmbH. This is an open access article under the terms of the Creative Commons Attribution-NonCommercial-NoDerivs License, which permits use and distribution in any medium, provided the original work is properly cited, the use is non-commercial and no modifications or adaptations are made.

DOI: 10.1002/adom.202001869

Table 1. Summary of available stimuli and respective adaptive polymer components to dynamically manipulate plasmonic nanoparticles and their clusters.

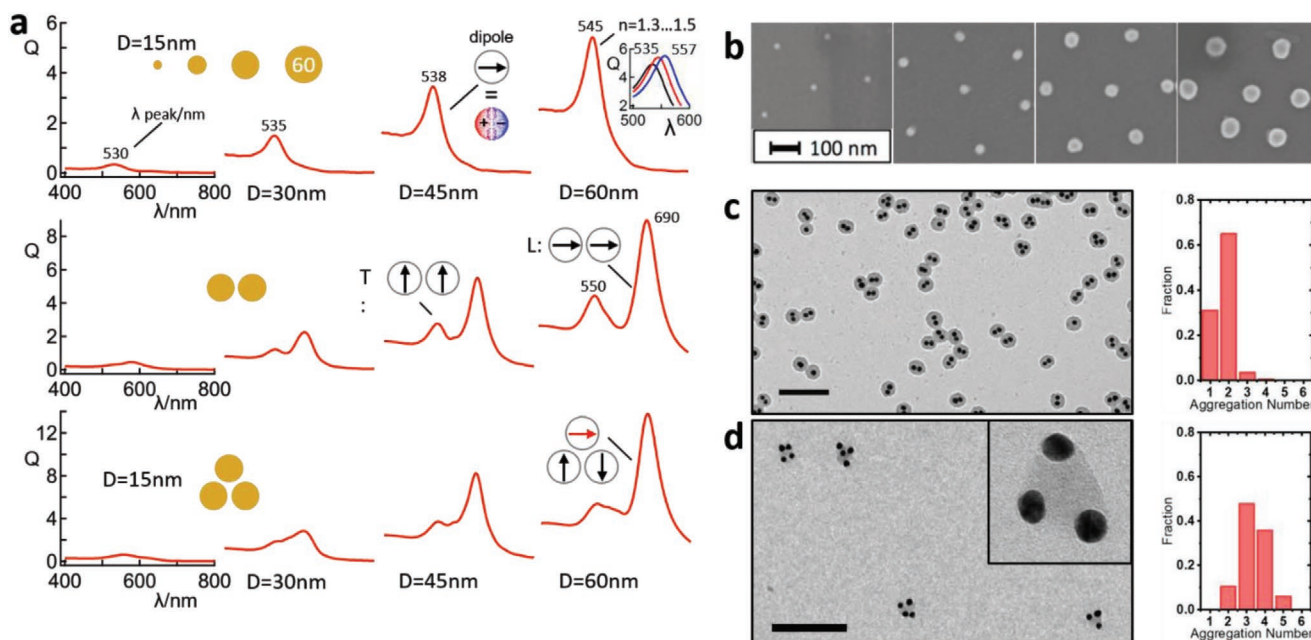
Stimulus/trigger	Active polymer component
Temperature	Poly(<i>N</i> -isopropylacrylamide); ^[15–20] polystyrene; ^[21,22] star block copolymers of poly(<i>N</i> -isopropylacrylamide) and poly(<i>N,N</i> -dimethylacrylamide); ^[23] poly(<i>N</i> -isopropylamide- <i>co</i> -allylactic acid); ^[24] poly[(di(ethylene glycol) ethyl ether acrylate- <i>co</i> -oligoethylene glycol acrylate)- <i>block</i> -(<i>N</i> -3-(dimethylamino)propyl methacrylamide)]; ^[25] poly(ethylene glycol) ^[26]
pH	Poly(aniline); ^[27–29] poly(allylamine); ^[30] poly(dimethylaminoethyl methacrylate); ^[31] poly(<i>N</i> -isopropylamide- <i>co</i> -allylactic acid) ^[24]
Redox reaction	Poly(aniline) ^[32,33,28]
Solvent environment	Polystyrene; ^[34–37] poly(styrene- <i>block</i> -(4-vinylbenzoic acid)); ^[38] poly(methyl methacrylate) ^[39]
Light	Spiropyran-containing poly(methacrylate); ^[40] azobenzene-containing poly(methacrylate); ^[41] block-copolymers with coumarin-containing poly(methacrylate) blocks ^[42]

2. Discussion

2.1. Homogeneous Plasmonic Clusters: Rational Design, Optical Properties, and Synthesis

Simulation methods have become indispensable in the rational design of cluster assemblies and the explanation of their optical properties. In order to complement, guide, and create transitions to the current discussion in literature, we have limited the simulation to gold/silver nanoparticles of different sizes and their assemblies in a homogeneous environment. The coherent coupling of light with the free electrons of the metallic NP can be introduced by the example of colloidal gold.^[43] For an individual particle, the optical parameters, such as spherical shape, gold material, and polymeric environment, are kept constant

and only the diameter (two times the radius) is changed (see **Figure 1**). This simplification corresponds to a common synthesis of gold nanoparticles,^[44,45] which enables their production in sufficient yield for a subsequent cluster formation. The refractive index $n = 1.4$ was set as the environment in order to mimic the desired functional environment. These simulations focus on the spectroscopic response (cross-section, SI units: m²), as these are quantitatively comparable with the results from commonly employed spectroscopic methods, such as UV–vis–NIR spectroscopy. Often, these spectroscopies are the first experimental characterizations performed after a synthesis. If only the size of an isolated particle is changed, the properties illustrated in **Figure 1a** can be obtained: With increasing size, the plasmonic resonance shifts to higher wavelengths (lower energy). Determined by the dielectric constant of the metal, the



free electrons of larger metal-nanoparticles can more easily be excited into oscillations (reflected in lower excitation energy).^[46] With the diameter selection between 15 and 60 nm, the commonly used sizes from the literature for clusters are covered and the plasmonic resonance occurs in the visible wavelength range. Furthermore, the cross-section amount of absorption and scattering increases with increasing size. In this article the simulated cross-section of the absorption and scattering is summed (extinction cross-section) and normalized by the area of the particle. This yields the extinction efficiency (Q) as a dimensionless quantity. This description is used throughout the progress report and allows a comparison of the different plasmonic clusters and thus a continuation of the current discussion in literature. It is important for the development into complex plasmonic clusters that a single particle can be approximated as a dipole.^[47] The simulations in this article can be reproduced using the finite-difference time-domain (FDTD) or Yee's method.^[48] In addition, the Mie theory by Mätzler^[49] was used to calibrate the results from using the FDTD method for an isolated particle.

In colloidal dispersion, the particles are stabilized by ligands (low molar mass surfactants, self-assembled monolayers or macromolecular ligands). In the present review, we focus on macromolecular ligands, which can be accounted for in the simulation by a dielectric shell. For an introduction, it is sufficient to assume a homogeneous dielectric environment. A simulated example with a 60 nm particle (inset Figure 1a) shows that the resonance shifts by 10 nm when the environment changes from water to a polymer ($\Delta n = 0.1$). For a detailed consideration of the resonance shift with different particle sizes, shell diameters and shell materials, we would like to refer to earlier work.^[50] This sensitivity, defined by the change in resonance wavelength divided by the change in the refractive index, can be increased by an arrangement in clusters.^[52,53] Nevertheless, the potential for modulating the plasmonic properties that comes with a functional shell should already be emphasized for an isolated particle, as this potential is also exploited in experimental systems. For example, the resonance wavelength of gold NPs coated with polyaniline (PANI) can be varied in a considerable wavelength range by adjusting the thickness of the PANI coating layer.^[54] Besides its static properties, a coating with macromolecular ligands can also provide adaptivity. By virtue of its composition and architecture, the polymer shell can enable active response to external stimuli. For example, dynamic core-shell type NPs can be realized, in which the polymer shell can be reversibly collapsed and expanded. When poly(*N*-isopropylacrylamide) (PNiPAAM) brushes are grafted onto gold NPs, shell collapse can be induced by plasmonic (local) heating of the gold core environment.^[15] Because the heating occurs only locally, the shell may rehydrate (expand) fast (≈ 100 ns) after stopping the illumination.^[16] A PNiPAAM coating of gold NPs thereby offers the possibility to thermally induce local refractive index changes leading to the described optical response.^[17]

The principle of reversibly re-configuring the polymer coating between two states has been exploited to create plasmonic switches. Here, gold NPs with poly(aniline) (PANI) shells are the most prominent example. In these PANI-coated gold NPs, the dielectric constant of the polymer shell can be modulated through pH^[27] and electrochemical^[32,33] triggers or a combination of both,^[28] since PANI inherently features

dual-stimuli responsive properties. In the case of redox (electrochemical) switching, the LSPR position can be precisely adjusted by controlling the potential, and high reversibility (200 cycles) could be achieved.^[32] For both stimuli, the extent to which the plasmon resonance maximum is switched is correlated with the PANI shell thickness.^[27,55] Comparably large plasmon resonance shifts (up to ≈ 150 nm)^[32] have been realized in this system, with high modulation depths.^[27] As such, these hybrid NPs have been used as a sensor to detect analytes that together with an assay lead to solution pH change.^[30]

By arranging two particles into a dimer cluster, the extinction efficiency can be increased and, even more importantly for applications, the plasmonic modes will undergo a qualitative change (Figure 1a). Due to the geometric arrangement in relation to the exciting electric field, a transverse (T) and a longitudinal (L) mode are generated. The longitudinal mode or the parallel alignment of the plasmonic dipoles along the geometric axis is the most dominant and energetically lowest mode. Theoretically, an antiparallel case is also excited. This antiparallel mode is also named dark mode because the sum of the dipole moments is zero and thus this mode cannot be excited from the far field. Moreover, this mode must be located for gold particles at much higher energy ($\ll 530$ nm) than the isolated particle resonance (plasmon hybridization).^[3] The transversal mode (T) can also be excited by an electric field component perpendicular to the geometric axis. The antiparallel arrangement of the dipoles is also called dark mode in the literature, because the individual dipoles cancel each other out.^[56] As a trade-off between computational effort and yield, only the modes parallel and perpendicular to the geometric axis are calculated (Figure 1). Moreover, in the case of dimers, the extinction efficiency increases when the particle diameter is increased, while the particle spacing (2 nm) is kept constant. At this point, it should be added that the observed redshift is a function of the ratio of distance to diameter. This general scaling behavior is also known as plasmon ruler equation.^[57]

If another particle is added, a trimer is created. The spectra of a dimer and a trimer are similar in their shape but they are completely different in their plasmonic modes. These modes can also be explained by a plasmon hybridization model.^[58] The plasmon hybridization can be built up by a linear combination of basic plasmonic modes of known geometries. In the case of a dimer, the model consists of two dipolar modes that can be developed into a parallel and an antiparallel mode as discussed earlier. Applied to a trimer, this model can be developed by a dipolar (red arrow in Figure 1a) and a quadrupolar mode (anti-parallel arranged dipoles).^[59] The fact that these hybridized modes typically show a higher quality factor than single particle LSPRs, is especially relevant for sensing applications,^[60] which motivated efforts to control complex cluster assemblies. The energetically highest mode can be explained by the single particle resonance. From a synthetic point of view, the formation of homogeneous plasmonic NP dimers and other discrete oligomers is challenging, because it requires the right balance between attractive NP interactions ensuring cluster formation and cluster stability (net attractive intra-cluster interactions) on one hand and colloidal stability of the resulting clusters on the other hand (net repulsive inter-cluster interactions or kinetic stability). Attractive directional NP interactions to form NP

dimers may be imparted through NP monofunctionalization.^[61] Thermodynamically controlled oligomer formation was realized in NPs decorated with a single polymer patch.^[38,34] Under poor solvency conditions, the polymer patches attract each other, leading to NP assembly driven by minimization of surface tension. At the same time, fusing individual polymer patches into a larger single patch invokes a chain stretching penalty. The balance of both contributions to the free energy may lead to the favored formation of discrete oligomers (trimers and tetramers, see Figure 1d).^[38] In addition, by relying on a diblock copolymer architecture of the surface-grafted macromolecules, the trimer/tetramer formation can be controlled via an external stimulus that specifically targets the outer, surface-remote polymer block.^[38] Kinetically controlled dimer formation in high yield ($\approx 60\%$) was realized in a reversible manner for gold NPs functionalized with mixed poly(methyl methacrylate)/poly(ethylene glycol) (PMMA/PEG) brushes, upon inducing PMMA brush collapse in a selective solvent.^[39] The assembly into dimers was attributed to the formation of mutually attractive collapsed PMMA domains. It was speculated that during NP encounter, the solvent-swollen PEG brushes would deplete from the forming dimer junction, and accumulate in the non-contacting areas, thus leading to dimer stabilization.^[39] For this system, it was shown theoretically that interparticle gap size can be controlled by adjusting the amount of grafted PMMA. Very small nanogaps (<1 nm) lead to the largest field enhancement in the nanogap.^[62] Note that at particle distances smaller than 2 nm, non-local and tunnel effects occur, which can be used for electron transport through the gap junction.^[63] A similar halt of NP agglomeration at the dimer state was also observed for gold NPs coated with a physisorbed layer of polystyrene-*block*-poly(acrylic acid) block copolymers at a moderately elevated solution temperature (60 °C, see Figure 1c).^[51] Here, control over the agglomeration process could be exerted by controlling the protonation state of the polyacid block. As can be seen from Figure 1a, dimerization of polymer-coated NPs leads to an additional longitudinal plasmon mode. Using the shift of this plasmon mode for sensing analytes leads to higher sensitivities compared with the transversal band.^[64] The peak position of the longitudinal band in dimers is also more sensitive to changes in the refractive index (induced by protonation of PANI-coating) compared with the monomeric case (see above).^[29] Light-induced reversible formation of oligomers of plasmonic NPs was realized for gold NPs coated with binary brushes consisting of spiropyran-containing poly(methacrylate) and poly(ethylene glycol) (PSPMA/PEG), which rests on the photoisomerization of spiropyran units in the polymer side chains of the PSPMA brushes into their conjugated, zwitterionic isomer upon UV irradiation.^[40] In this system, SERS activity can be modulated depending on the light-controlled dispersion state.

Heterodimers (of gold NPs of distinct dimension) have been realized through electrostatic assembly of oppositely charged nanoparticles. The dimer structures were stabilized—and prevented from fusing into larger assemblies—by stabilization with a densely grafted PEG layer.^[65] In another example, triblock copolymers made from a bifunctional reversible addition–fragmentation chain transfer (RAFT) agent, in which the RAFT trithiocarbonate group is located in the center of the middle (polystyrene) block, which joins two outer poly(acrylic

acid) blocks were used to template the formation of quantum dots.^[66] The as-prepared quantum dots were functionalized with polystyrene loops, which allowed subsequent attachment of (on average one) gold NPs at a certain distance from the quantum dot.^[67] These heterogeneous dimers showed significant fluorescence enhancement, which can be attributed to the distance-dependent balance in which near-field-promoted increased excitation rates overcompensate de-excitation pathways, thanks to the polystyrene spacer.

2.2. Transition from Tightly Packed to Chain Clusters and Clusters with Material Heterogeneity

Upon self-assembly, polymer-coated NPs can follow distinct scenarios, as addressed in a fundamental work of Kumacheva and co-workers.^[68] If charged polymer-grafted NPs are exposed to poor solvency conditions for the coating polymer layer, the balance between attractive (solvophobic) polymer– interactions and electrostatic repulsion can lead to either (3D) globular assemblies (governed by minimization of polymer–solvent interactions) or (1D) chain assemblies (governed by electrostatic repulsion). The spatial arrangement of plasmonic NPs in their superstructures plays a decisive role for their optical properties. This is highlighted in Figure 2a for the smallest cluster for which distinct spatial arrangements are conceivable, the trimer

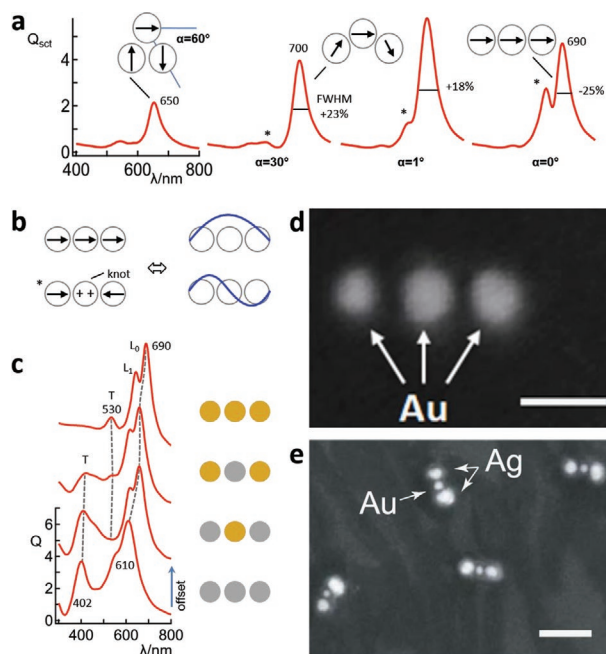


Figure 2. a) Simulated transition from a tightly packed trimer to a chain. The asterisk marks the first order chain mode, which is very sensitive to the orientation angle (α). b) Analogy between chain modes and the particle in the box model. c) Evolution of the optical properties for homogeneous and heterogeneous gold and silver trimer chains. d) Scanning electron microscopy image of a homogeneous gold trimer chain (scale bar is 50 nm). e) Scanning electron microscopy image of a heterogeneous silver-gold-silver trimer chain (scale bar is 100 nm). Adapted with permission.^[69] Copyright 2020, AAAS. Definition of abbreviations: scattering efficiency (Q_{sct}), wavelength (λ), full width at half maximum (FWHM).

cluster. The plasmonic modes of a tightly packed trimer and a trimer chain differ fundamentally. Therefore, this transition in optical extinction spectra could be used to monitor the dynamic re-arrangement of trimer structures that gradually approach their (linear) equilibrium structures.^[69] Furthermore, it can be speculated that the D_{3h} -to- $D_{\infty h}$ (or vice versa) transition may be realized with an adaptive polymer. To do this, the position of the central NP must be fixed while the others can change their position like satellites in orbit. This scenario was calculated with gold NPs with a diameter of 45 nm (spacing 2 nm) with orientation angles (α) between 60° and 0° . From these calculations, the following observations can be made: During the transition to the chain ($60^\circ < \alpha < 0^\circ$), the energetically lowest mode shifts to the red. In this transition, the resonance becomes wider and the scattering efficiency increases. If the particles are in a line ($\alpha = 0^\circ$), the chain modes of zero-order and first-order can be identified. In the line assembly the plasmonic modes are clearly sharper compared with the modes during the transition. Note, in this simulation we consider the scattering properties of the excited plasmon modes only. In the case of 0° , the zero-order and first-order of the chain mode are solely excited, which scatter less into the far field than at 1° . The chain modes can be developed from a particle in the box model.^[70–72] For this purpose, the potential well is developed by a discrete number of coupled dipoles. Thus, along the chain (potential) can exist only modes which are an integer multiple of its half wavelength. Moreover, the simulations also show that the chain mode of the first order is more sensitive by a factor of two to changes in the orientation angle compared to the zero order. These first-order chain modes (or antisymmetric/dark mode) are also suitable for efficient energy transport along the geometric axes.^[73,74]

In Figure 2c, the impact of the nature of the metal is illustrated by comparing gold trimers with silver trimers as well as mixed cases. The dashed line indicates that the plasmonic modes are maintained for the selected material combinations. If one compares the pure gold chains with the pure silver chains one can observe a shift of all modes to higher energies. This can be attributed to the different electron density for silver and gold.^[75] Thus, in the case of silver, the visible part of the electromagnetic spectrum can be covered completely by plasmonic modes. Furthermore, the simulations show the lower damping advantage of silver in the wavelength range from 300 to 515 nm.^[14] On the other hand, the lower damping advantage of gold can be seen in the wavelength range between 515 and 800 nm. In this range, the resonance quality defined by the frequency-to-bandwidth ratio is much narrower when gold is present. The calculations were performed on 45 nm-sized particles at a distance of 2 nm and an unpolarized light excitation. It should also be noted that these heterostructures can be used for energy transport with low losses.^[76] In relation to applications, the material must be considered in order to match the desired wavelength range, optical quality, and chemical stability.

Both the homogeneous as well as the heterogeneous trimer chains can be realized experimentally by a new supracolloidal synthesis paradigm, which is the self-limiting directional nanoparticle bonding.^[69] This concept lies on the salt-bridge formation between an inner poly-acid polymer block of a diblock terpolymer grafted onto one type of NPs and an inner poly-base block of a complementary diblock terpolymer grafted on another

type of NPs. For both cases, an outer, surface-remote PEG-block serves to provide colloidal stability of the derived self-assembled clusters. Depending on the number of acid/base functionalities on each of the NPs, interparticle bonding ceases once all acid/base functionalities are consumed in their neutralization reaction, leading to controlled cluster sizes. The bonding angles are governed by electrostatic repulsion between the charged groups in the salt bridges that constitute the interparticle bonds. Thus, for trimer clusters, an equilibrium bonding angle of 180° (corresponding to $\alpha = 0^\circ$, Figure 2a) results.

Larger chain assemblies of plasmonic NPs (with a dispersion with respect to the number of constituent NPs) have also been realized. Cetyltrimethylammonium bromide (CTAB) coated gold nanorods (NRs) may be site-selectively functionalized with polymer ligands at the NR tips.^[35,36] Upon reducing the solvent quality for the polymer ligands, the polymer-coated NR tips become mutually attractive, and this may result in the formation of chains of gold NRs. Interestingly, the gold NR gap distance can be manipulated in response to the solvent environment: Poorer solvency conditions lead to the accumulation of more polymer ligands in the inter-rod gaps and hence larger separation.^[35] Such AuNR chains have been used for hot-spot-driven SERS and the enhancement effect was found to increase with increasing the number of AuNRs per chain^[37] and decreasing gap size.^[77] It is also possible to equip these AuNR chains with chain-end functionality by employing colloidal chain stoppers.^[78] By decorating the AuNR tips with PNⁱPAAM, a reversible photothermal chain assembly of AuNRs can be achieved.^[79] Chain-assemblies of spherical gold NPs can be created by using diblock copolymer as template.^[80] Depending on the surface chemistry of the NPs, cylindrical micelles with NPs incorporated in the micelle center may be obtained.^[80] In another system comprising gold NPs coated with poly(dimethylaminoethyl methacrylate) (PDMAEMA), the formation of chains of spherical gold NPs could be triggered by changing the solution pH.^[31] Heterogeneous chain assembly systems include binary (comprising two distinct metal NPs) block-copolymer-type^[81,82] as well as alternating-copolymer-type^[65,83,84] chains. Here, the alternating structure may be realized by relying on oppositely charged nanoparticle building units.^[83]

2.3. Controlled Agglomeration of Equally Sized Plasmonic Nanoparticles

The assembly of plasmonic nanoparticles into larger, globular assemblies^[85–87] can be used for different purposes, including the shift of the plasmon resonance peak as well as for colorimetric assays for the detection of specific analytes. The former process can be controlled by adjusting the ratio between a stabilizing polymer coating and another (small molecule) destabilizing agent (see Figure 3a).^[88] Starting from spherical primary gold NPs, enhanced absorbance in the near-IR tissue transparency window (a wavelength range in which electromagnetic radiation can penetrate comparably deep into biological tissue), can be achieved upon aggregation.^[88] The extent of cluster formation can as well be controlled by external triggers which address a functional polymer coating, for instance by adjusting temperature^[21,22] and by applying light.^[41,42] Coumarin-containing

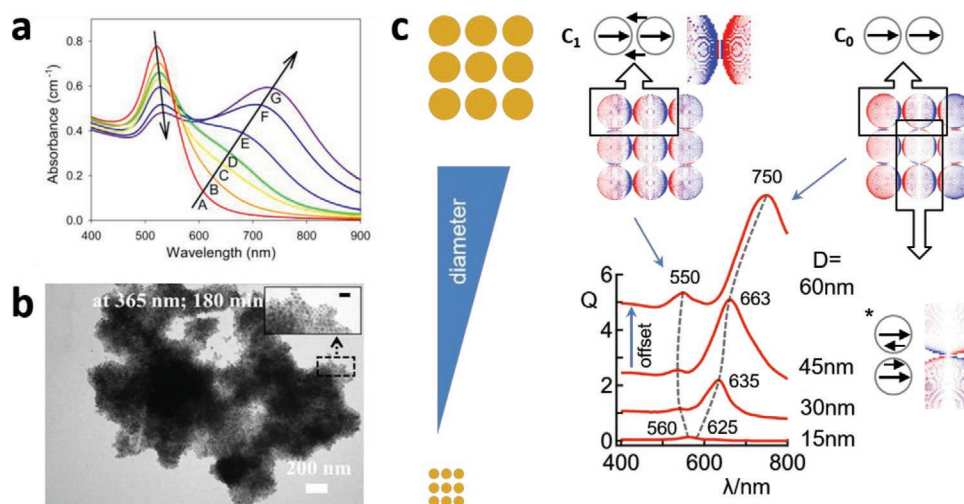


Figure 3. a) Measured optical response upon controlled aggregation of 15 nm polymer-coated gold NPs. The extent of cluster formation increases from A to G. Adapted with permission.^[88] Copyright 2013, American Chemical Society. b) (Reversibly) photo-crosslinked aggregates of gold NPs functionalized with coumarin-containing polymers.^[42] Adapted with permission.^[42] Copyright 2018, NAS USA. c) Simulation of a nonamer cluster at different particle sizes and constant particle spacing (2 nm). The surface charges show the cluster mode zero (C_0) and first order (C_1). The boxes with arrows show schematic drawings of the dipoles and an enlargement of the surface charges at the contact point.

polymer ligands for example can be used for photochemical NP crosslinking (via [2+2]-cycloaddition reaction) and the cluster dis-assembly (via cycloreversion at higher photon energies).^[42]

By virtue of the plasmonic properties of the clusters, colorimetric assays can be implemented through linear macromolecules that are anchored to the plasmonic nanoparticle by one chain end, and possess a recognition element for the analyte on the other, surface-remote chain end. Depending on the architecture of the polymeric coating layer, these nanoparticles may or may not aggregate upon analyte binding.^[89] In the former case, the associated plasmon mode shift can serve as an optical read-out of analyte concentration. In many cases such design benefits from multivalency effects,^[90] since multiple recognition elements are expressed on the exterior of the consequently-produced NP coating layer.^[91,92] Recently, Gibson and co-workers implemented dynamic features to this kind of colorimetric assay, by developing systems with externally triggerable recognition element representation.^[93,94] Their concept builds on earlier work by Mirkin and co-workers^[95] and rests on thermoresponsive PNⁱ-PAAM, which was used to shield the recognition elements below its lower critical solution temperature (LCST) and expose them above its LCST, thereby “gating” the sensor capabilities.

In the experimental systems discussed above, the globular assemblies of plasmonic NPs usually involve a dispersion with respect to the number of NPs per clusters. To understand key features of the plasmonic properties of these clusters, we exemplarily studied an arrangement of nine NPs (nonamer) into a tight packing. Such exemplary considerations are also useful to describe the transition from a nonamer cluster to a core-satellite cluster, as will be of importance later. At this point, this observation provides an insight into the mode structure of plasmonic clusters. The simulated spectra show that the energetically lowest cluster mode (C_0) shifts disproportionately strong red (25%) when the particle diameter is increased fourfold. Note that the cluster mode of a nonamer (663 nm @ $D = 45$ nm) differs from the chain mode of a trimer (690 nm,

see Figure 2a). The surface charges in Figure 3c show that additional mirror charges occur at the vertical contact points. Energy is necessary to induce these mirror charges, therefore the nonamer cluster mode is blue-shifted compared with the trimer chain mode. The first order cluster mode (C_1) shows a different behavior. This C_1 mode is easier to excite for smaller particles (C_1 : 560 nm @ $D = 15$ nm) compared with larger particles (C_1 : 550 nm @ $D = 60$ nm). Note that a single plasmon decays either into a single photon (scattering) or into an electron-hole pair (absorption). For large particles, the probability increases that the photons are scattered. This behavior can be explained by the scatter to extinction ratio also known as scattering performance.^[96] For these decay channels, the energy is taken from the exciting field, therefore the C_1 mode for small particles is slightly red-shifted compared with the C_1 mode for large particles. When comparing the cluster modes with the chain modes, the following must be added: First, the quality of the modes is lower with cluster modes. Second, the energetic distance between the zero-order and first-order modes is larger for cluster modes. Third, the mode structure is different. These observations have concrete consequences for the application when the transition from a chain to a cluster is induced.

2.4. Plasmonic Clusters with Size Heterogeneity: Core-Satellite Clusters and Their Functionalities

The nonamers are suitable to model the transition from homogeneous to heterogeneous clusters with different sizes (see Figure 4). With this approach, core-satellite clusters can be viewed in a 2D plane. This procedure simplifies the description of the plasmonic modes, because the surface charge oscillations always propagate in one plane. In a subsequent step, the plasmonic modes discussion can be extended to a cluster with particles in all directions in space (3D). Due to the symmetric geometry of the core-satellite clusters, it is sufficient to calculate

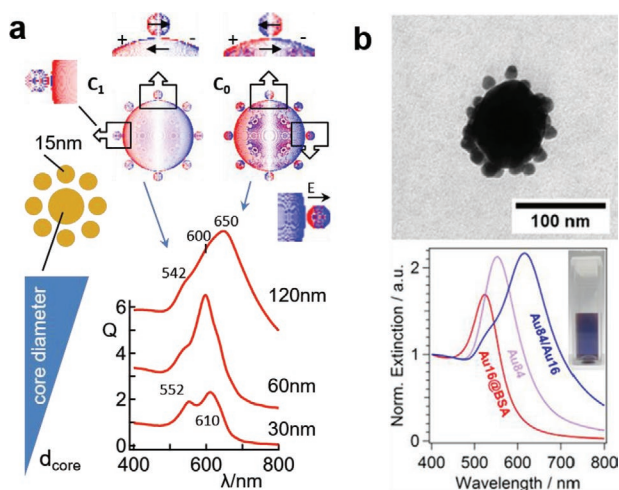


Figure 4. a) Simulation of a core–satellite cluster in 2D (nanometer) at constant satellite size and varying core diameter (d_{core}). The core–satellite distance is 2 nm. The surface charges show the cluster mode zero (C_0) and first order (C_1). The boxes with arrows show schematic drawings of the dipoles and an enlargement of the surface charges at the contact point. b) TEM and optical extinction spectrum of core–satellite clusters, mediated by protein (BSA) linker comprising gold cores (84 nm) and on average 35 gold satellites (16 nm) with an interparticle distance of 4 nm.^[98] (Adapted with permission.^[98] <https://pubs.acs.org/doi/10.1021/acsnano.5b07533>, further permissions related to the material excerpted should be directed to the ACS).

the cluster at one polarization only. The extinction spectrum of such clusters—with its two characteristic peaks—are similar to that of a dimer (Figure 4a). In a plasmonic cluster with various sizes, however, the main difference is that one particle can excite or attenuate the other. As previously mentioned, induced charges are generated at the contact surfaces (Figure 3c). In a particle-to-film coupled setup this effect can also be viewed individually.^[97] This behavior observed in Figure 4a occurs at the first order cluster mode (C_1 ; 542 nm). It should be noted that at the C_1 mode, the core is also excited. The resonance wavelength of a $D = 120$ nm gold NP is at 600 nm with an FWHM of 200 nm.^[3] An opposite behavior, excitation of the core particle, is observed at the energetically lowest mode (C_0). At this mode, the core induces the oppositely directed surface charge in the satellite particle. Furthermore, the C_0 mode is energetically lower than the single particle resonance of the core. This behavior can be explained by the coherent coupling between the core and the satellite particles. This mode structure also continues for smaller core particle diameters. For applications, the strength of the field enhancement is crucial. The surface charges are derived from the calculations of the electric fields. The magnitude of these field peaks will be discussed next. At this point, it should be noted that for applications the cluster mode is tailored by the choice of NP size, distance, number, and position.

The small (few nm) nanogaps in core–satellite type structures as emphasized in Figure 4 are sought after in processes that benefit from high field enhancement in these hot-spot-dominated systems,^[98] such as SERS^[99–103] and plasmonic heating.^[102] The coupling interaction between the core and satellite NPs can also be used for refractive index sensing, as

this assembly structure is more sensitive to refractive index changes than are the isolated core or satellite particles.^[53] The modular combination of plasmonic building units with distinct dimension and shape enables the engineering of the plasmon coupling and the plasmon resonance wavelength.^[102,103] Such nanoclusters can lead to Raman enhancement factors which are high enough to allow spectrum collection from single clusters.^[101] Recently, an intricate strategy was developed by which satellite NPs can be positioned selectively at the high curvature hot-spot regions of non-centrosymmetric NPs.^[104] This strategy employs the site-selective constrained de-wetting of nanoparticles end-grafted with polymer ligands,^[34,105] and subsequent functionalization of vacant (polymer-deprived) surface regions. That way, plasmonic satellite NPs can be selectively attached to, for example, the vertices of nanocubes and triangular nanoprisms.^[104]

Abiding effort was recently dedicated to control the distance between the core and the satellites, both in static systems as well as in dynamic systems. Simulations (Figure 5a) show that at a distance of 32 nm there is almost no coupling remaining. The resonance observed at 536 nm is close to the resonance of a 15 nm particle (530 nm). At smaller distances a red-shift of the resonance can be observed, which can be attributed to plasmonic coupling. The resonance shifts by 24 nm to lower energy when the distance is reduced from 32 to 4 nm. To achieve the same redshift with an isolated particle resonance, the diameter would have to be increased seven times (from 15 to 100 nm). A significant change in the extinction spectrum only occurs when the core–satellite distance reaches 2 nm. At this distance a distinction can be made between a cluster mode of zero (610 nm) and first order (560 nm). In addition, the intensity of the electric field was calculated for the energetically lowest modes at two configurations. These calculations show that the field intensity is 20 times higher at a distance of 2 nm compared to a distance of 32 nm. These local field enhancements also known as hotspots and their benefits for spectroscopic applications such as SERS as discussed above. Experimentally, the control of interparticle spacing in static systems becomes possible with surface-grafted macromolecules. That way, the gap size can be adjusted between a few nm up to several tens of nm (see Figure 5b), both for systems comprising gold NPs of distinct sizes,^[99,106,107] as well as for binary systems with gold NP core and silver NP satellites.^[108] The dynamic modulation of the interparticle gap size becomes possible by using adaptive polymeric linkers.^[18,19,23,25] In the majority of works, this stimulus-responsive interparticle distance modulation was achieved by relying on the LCST behavior of PNIPAAm (Figure 5c).^[18,19,23] In addition, double responsive structures that respond to both heating above a LCST as well as cooling below an upper critical solution temperature (UCST), were realized through diblock copolymer linkers comprising one UCST-type and one LCST-type thermoresponsive block.^[25] In temperature intervals away from critical temperatures, the temperature-dependent swelling of polymer brushes can be used to gradually change interparticle spacings. In core–satellite systems comprising gold core and quantum dot satellites, this can be used for temperature-dependent fluorescence modulation, that is, a nanoscale thermometer.^[26]

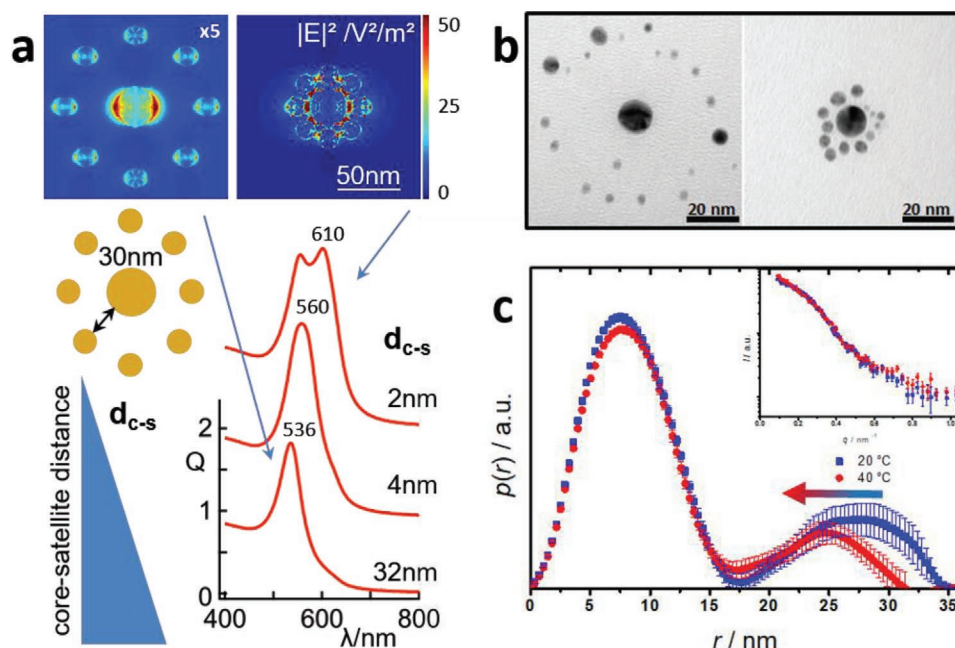


Figure 5. a) Calculated electric field intensity and extinction at 32 and 2 nm core-satellite distances. Displayed is the average field intensity in beam direction. Electric field intensity for 32 nm must be multiplied by a factor of 5 to match the scale bar. b) Core-satellite clusters with varying core-satellite distance as a function of the degree of polymerization of the linking star polymer (static system).^[106] Adapted with permission.^[106] Copyright 2014, Wiley-VCH. c) Dynamic switching of the core-satellite distance upon heating above the LCST of inner poly(NiPAAM) blocks of the linking star polymer as determined by SAXS.^[23] Adapted with permission.^[23] Copyright 2018, American Chemical Society.

2.5. Toward Colloidal Metamaterials

Metamaterials feature properties not typically encountered in nature.^[109] The most famous properties are negative refractive index,^[110] electromagnetic cloaking,^[111] or strong circular dichroism.^[112] Large-scale synthesis of plasmonic nanoparticles and their self-assembly into clusters can solve the scaling challenge of metamaterials at reasonable costs. In addition to electric field amplifications, magnetic field enhancements also occur in certain cluster geometries. In the simplest case, this occurs in a single satellite that couples with the core. This concept was demonstrated by the Linden group in an analogous setup with two plate pairs metallic nanostructures.^[113] Such structures possess the electrical and magnetic modes, which are necessary for the metamaterial property. By controlling the number of surrounding satellites as well as the core material in core-satellite-type clusters, colloidal metafluids, that is, plasmonic supercolloids that feature optical properties that go beyond the characteristics discussed so far, may be accessed. Synthetically, the number of satellites can be precisely adjusted up to moderate satellite numbers through the very recently established concept of self-limiting directional nanoparticle bonding.^[69] This work was already discussed in the context of linear plasmonic trimers above, but depending on the ratio of reactive (acid and base) groups on the complementary plasmonic NPs, a wider range of satellite numbers can be precisely adjusted as well (see **Figure 6a**). Because the inter-NP junctions are rich with charged groups, electrostatic repulsion interactions of these junctions lead to a symmetrical equilibrium arrangement of the satellite NPs. When larger satellite numbers are targeted, this parameter may be controlled by adjusting the feed ratio to the core

particle in the cluster formation process.^[18] This of course leads to a comparably broad satellite number distribution.

If the core is replaced by a non-metal dielectric material, only the satellite particles may plasmonically couple. Note that coupling between two gold nanoparticles occurs when they are less than 2.5 times their diameter apart.^[116] As a result of this coupling interaction, it was shown in the working group of Dionne that silver satellites assembled around a dielectric (polystyrene) core can create ring current.^[114] Similar behavior was observed for gold nanoparticles assembled around a silica core.^[115] These ring currents with their magnetic moment are a prerequisite for the formation of so-called metafluid.^[117] For comparison, this calculation was added in the **Figure 6b** for a dielectric core ($n = 1.4$). By assembling the plasmonic nanoparticles on the surface of PNiPAAM-brush-coated silica NPs, PNiPAAM microgel particles,^[20] or poly(NiPAAM-co-allylactic acid) microgel particles,^[24] the dielectric core becomes thermally responsive^[18,20] or pH/temperature dual responsive,^[24] in addition, which allows reversible swelling/shrinking transitions of the overall assembly structure, thereby altering also the inter-satellite spacings.^[18,20,24]

3. Summary and Future Prospects

The plasmonic properties of individual plasmonic NPs are well understood. When these individual entities are arranged in clusters, a rich phenomenology in their optical behavior results. This can be studied in computer simulations, as we have done in this progress report. The cluster properties are controlled through the combination of constituent NPs, but also the cluster

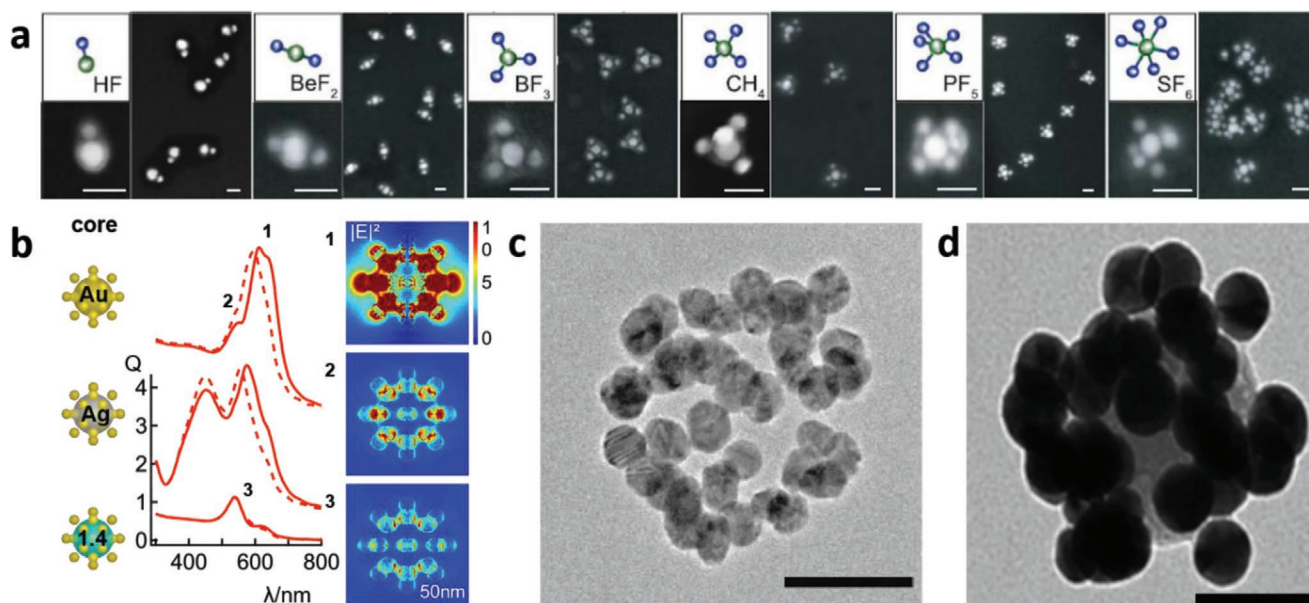


Figure 6. a) Symmetric arrangement of core-satellite clusters with defined satellite number, mimicking the symmetry of small molecule coordination polyhedra.^[69] Adapted with permission.^[69] Copyright 2020, AAAS. b) Left: Calculated spectra for a core-satellite cluster with the core materials gold, silver and polymer ($n = 1.4$) as well as for a core-satellite distance of 2 nm (solid line) and 4 nm (dashed line). Right: Electric field intensity for selected modes. The core diameter is 60 nm and the diameter of the 26 satellites is 15 nm. c) Silver NPs assembled around polystyrene beads.^[114] Adapted with permission.^[114] Copyright 2013, American Chemical Society. d) Gold NPs assembled around silica NPs.^[115] Adapted with permission.^[115] Copyright 2015, American Physical Society. The scale bars are 50 nm in (a) and (d) and 100 nm in (c).

architecture. To date, this cluster architecture can be tailored using synthetic polymers. Their use enables the synthesis of supracolloidal systems of reasonable complexity. Moreover, the soft polymer component may be used to implement adaptive properties, and, by virtue of this, add another dimension to the plasmonic properties of NPs and their clusters. Depending on the chemical nature of the employed polymers, a range of stimuli can be used to dynamically manipulate the arrangement structure of plasmonic NP clusters, and hence their optical properties. In typical examples, this is realized through external stimuli that lead to a gradual or sharp polymer conformational transition at a given temperature, pH, solvent environment, etc.

Less attention was so far drawn to systems with multiple levels of stimulus responsiveness. Such systems may include multiple-stimuli responsivities (as discussed in this progress report for dual responsive systems)^[24,28] and/or hierarchical stimulus responsive behavior, that is, “staged” responsivity toward distinct orthogonal stimuli.^[38] Further advances in this regard may lead to a new generation of “smart” materials, which goes beyond the switching between two distinct states and involves more complex cascade adaptive behavior. Also, the systems reported to date and discussed in this contribution rely on adaptive control through external stimuli, however, in principle internal feedback loops may be realized in similar systems as well. Implementation of this may lead to new paradigms for optical systems, which feature self-regulation, self-activation, or complex conformational changes on the single cluster level. The latter is especially of interest for colloidal polymers consisting of $\gg 10$ individual particles since here the conformational space is much larger and conformational changes may dramatically influence coupling properties as

well as accessibility of reactive centers for photocatalytic reactions. Further, combining multiple cluster types may facilitate complex cascades in shape changes/reactions. This provides tantalizing opportunities, for example, in the fields of sensing and photocatalysis, in which a new generation of multiplexed sensor materials as well as self-adaptive photocatalytic systems can be foreseen. Thus, supracolloidal structures may ultimately approach biological examples like enzymes or motor proteins in their functionality.

Acknowledgements

C.R. acknowledges receipt of a Liebig fellowship (Fonds der Chemischen Industrie). This project was financially supported by the Volkswagen Foundation through a Freigeist Fellowship to T.A.F.K. A.F. acknowledges German Science foundation for funding within DFG project DFG Fe 600 34-1.

Open access funding enabled and organized by Projekt DEAL.

Conflict of Interest

The authors declare no conflict of interest.

Keywords

electromagnetic simulations, nanomaterial synthesis, plasmonics, self-assembly, supracolloidal

Received: October 29, 2020

Revised: January 11, 2021

Published online: February 8, 2021

- [1] M. Mayer, A. M. Steiner, F. Röder, P. Formanek, T. A. F. König, A. Fery, *Angew. Chem., Int. Ed.* **2017**, *56*, 15866.
- [2] G. Haberkühner, F. P. Schmidt, G. Schaffernak, A. Hörl, A. Trügler, A. Hohenau, F. Hofer, J. R. Krenn, U. Hohenester, G. Kothleitner, *Nano Lett.* **2017**, *17*, 6773.
- [3] V. Myroshnychenko, J. Rodríguez-Fernández, I. Pastoriza-Santos, A. M. Funston, C. Novo, P. Mulvaney, L. M. Liz-Marzán, F. J. García de Abajo, *Chem. Soc. Rev.* **2008**, *37*, 1792.
- [4] W. Xie, B. Walkenfort, S. Schlücker, *J. Am. Chem. Soc.* **2013**, *135*, 1657.
- [5] T. G. W. Edwardson, K. L. Lau, D. Bousmail, C. J. Serpell, H. F. Sleiman, *Nat. Chem.* **2016**, *8*, 162.
- [6] L. Lermusiaux, A. Sereda, B. Portier, E. Larquet, S. Bidault, *ACS Nano* **2012**, *6*, 10992.
- [7] C. Rossner, A. Fery, *MRS Commun.* **2020**, *10*, 112.
- [8] M. A. C. Stuart, W. T. S. Huck, J. Genzer, M. Müller, C. Ober, M. Stamm, G. B. Sukhorukov, I. Szleifer, V. V. Tsukruk, M. Urban, F. Winnik, S. Zauscher, I. Luzinov, S. Minko, *Nat. Mater.* **2010**, *9*, 101.
- [9] G. Moad, *Polym. Chem.* **2017**, *8*, 177.
- [10] D. Lu, J. Zhou, Y. Chen, J. Ma, H. Duan, *Macromol. Rapid Commun.* **2019**, *40*, 1800613.
- [11] C. Yi, Y. Yang, B. Liu, J. He, Z. Nie, *Chem. Soc. Rev.* **2020**, *49*, 465.
- [12] Y. Yang, C. Gu, J. Li, *Small* **2019**, *15*, 1804177.
- [13] M. Blanco-Formoso, N. Pazos-Perez, R. A. Alvarez-Puebla, *Nanoscale* **2020**, *12*, 14948.
- [14] M. Mayer, M. J. Schnepf, T. A. F. König, A. Fery, *Adv. Opt. Mater.* **2019**, *7*, 1800564.
- [15] M. J. Penelas, C. B. Contreras, P. C. Angelomé, A. Wolosiuk, O. Azzaroni, G. J. A. A. Soler-Illia, *Langmuir* **2020**, *36*, 1965.
- [16] S. Murphy, S. Jaber, C. Ritchie, M. Karg, P. Mulvaney, *Langmuir* **2016**, *32*, 12497.
- [17] R. Contreras-Cáceres, A. Sánchez-Iglesias, M. Karg, I. Pastoriza-Santos, J. Pérez-Juste, J. Pacífico, T. Hellweg, A. Fernández-Barbero, L. M. Liz-Marzán, *Adv. Mater.* **2008**, *20*, 1666.
- [18] L. Wu, U. Glebe, A. Böker, *Adv. Mater. Interfaces* **2017**, *4*, 1.
- [19] F. Han, S. R. C. Vivekchand, A. H. Soeriyadi, Y. Zheng, J. J. Gooding, *Nanoscale* **2018**, *10*, 4284.
- [20] M. Karg, I. Pastoriza-Santos, J. Pérez-Juste, T. Hellweg, L. M. Liz-Marzán, *Small* **2007**, *3*, 1222.
- [21] K. Serrano, M. S. , T. A. F. König, J. S. Haataja, T. I. Löbbling, H. Schmalz, S. Agarwal, A. Fery, A. Greiner, *Macromol. Rapid Commun.* **2016**, *37*, 215.
- [22] H. Tao, E. Galati, E. Kumacheva, *Macromolecules* **2018**, *51*, 6021.
- [23] C. Rossner, O. Glatter, P. Vana, *Macromolecules* **2017**, *50*, 7344.
- [24] M. Karg, Y. Lu, E. Carbó-Agibay, I. Pastoriza-Santos, J. Pérez-Juste, L. M. Liz-Marzán, T. Hellweg, *Langmuir* **2009**, *25*, 3163.
- [25] F. Han, A. H. Soeriyadi, J. J. Gooding, *Macromol. Rapid Commun.* **2018**, *39*, 1800451.
- [26] J. Lee, A. O. Govorov, N. A. Kotov, *Angew. Chem., Int. Ed.* **2005**, *44*, 7439.
- [27] N. Jiang, L. Shao, J. Wang, *Adv. Mater.* **2014**, *26*, 3282.
- [28] J. W. Jeon, J. Zhou, J. A. Geldmeier, J. F. Ponder, M. A. Mahmoud, M. El-Sayed, J. R. Reynolds, V. V. Tsukruk, *Chem. Mater.* **2016**, *28*, 7551.
- [29] N. Jiang, Q. Ruan, F. Qin, J. Wang, H. Q. Lin, *Nanoscale* **2015**, *7*, 12516.
- [30] G. K. Joshi, M. A. Johnson, R. Sardar, *RSC Adv.* **2014**, *4*, 15807.
- [31] H. Xia, G. Su, D. Wang, *Angew. Chem., Int. Ed.* **2013**, *52*, 3726.
- [32] W. Lu, N. Jiang, J. Wang, *Adv. Mater.* **2017**, *29*, 1604862.
- [33] T. A. F. König, P. A. Ledin, J. Kerszulis, M. A. Mahmoud, M. A. El-Sayed, J. R. Reynolds, V. V. Tsukruk, *ACS Nano* **2014**, *8*, 6182.
- [34] R. M. Choueiri, E. Galati, H. Thérien-Aubin, A. Klinkova, E. M. Larin, A. Querejeta-Fernández, L. Han, H. L. Xin, O. Gang, E. B. Zhulina, M. Rubinstein, E. Kumacheva, *Nature* **2016**, *538*, 79.
- [35] Z. Nie, D. Fava, E. Kumacheva, S. Zou, G. C. Walker, M. Rubinstein, *Nat. Mater.* **2007**, *6*, 609.
- [36] K. Liu, Z. Nie, N. Zhao, W. Li, M. Rubinstein, E. Kumacheva, *Science* **2010**, *329*, 197.
- [37] A. Lee, G. F. S. Andrade, A. Ahmed, M. L. Souza, N. Coombs, E. Tumarkin, K. Liu, R. Gordon, A. G. Brolo, E. Kumacheva, *J. Am. Chem. Soc.* **2011**, *133*, 7563.
- [38] C. Rossner, E. B. Zhulina, E. Kumacheva, *Angew. Chem., Int. Ed.* **2019**, *58*, 9269.
- [39] L. Cheng, J. Song, J. Yin, H. Duan, *J. Phys. Chem. Lett.* **2011**, *2*, 2258.
- [40] L. Zhang, L. Dai, Y. Rong, Z. Liu, D. Tong, Y. Huang, T. Chen, *Langmuir* **2015**, *31*, 1164.
- [41] D. Huebner, C. Rossner, P. Vana, *Polymer* **2016**, *107*, 503.
- [42] Y. Chen, Z. Wang, Y. He, Y. J. Yoon, J. Jung, G. Zhang, Z. Lin, *Proc. Natl. Acad. Sci. USA* **2018**, *115*, E1391.
- [43] M. X. Faraday, *Philos. Trans. R. Soc. London* **1857**, *147*, 145.
- [44] N. G. Bastús, J. Comenge, V. Puntès, *Langmuir* **2011**, *27*, 11098.
- [45] Y. Zheng, X. Zhong, Z. Li, Y. S. Xia, *Part. Part. Syst. Charact.* **2014**, *31*, 266.
- [46] K. M. Mayer, J. H. Hafner, *Chem. Rev.* **2011**, *111*, 3828.
- [47] P. Mulvaney, *Langmuir* **1996**, *12*, 788.
- [48] Lumerical Inc., CA, <https://www.lumerical.com/Products/Fdtd/> (accessed: August 2020).
- [49] C. Mätzler, *IAP Res. Rep.* **2002**, *8*, 9.
- [50] M. B. Müller, C. Kuttner, T. A. F. König, V. V. Tsukruk, S. Förster, M. Karg, A. Fery, *ACS Nano* **2014**, *8*, 9410.
- [51] X. Cheng, G. Zhao, Y. Lu, M. Yan, H. Wang, H. Chen, *Chem. Commun.* **2018**, *54*, 7746.
- [52] T. König, R. Kodiyath, Z. A. Combs, M. A. Mahmoud, M. A. El-Sayed, V. V. Tsukruk, *Part. Part. Syst. Charact.* **2014**, *31*, 274.
- [53] J. Prasad, I. Zins, R. Branscheid, J. Becker, A. H. R. Koch, G. Fytas, U. Kolb, C. Sönnichsen, *J. Phys. Chem. C* **2015**, *119*, 5577.
- [54] H. Hou, L. Chen, H. He, L. Chen, Z. Zhao, Y. Jin, *J. Mater. Chem. B* **2015**, *3*, 5189.
- [55] J. W. Jeon, P. A. Ledin, J. A. Geldmeier, J. F. Ponder, M. A. Mahmoud, M. El-Sayed, J. R. Reynolds, V. V. Tsukruk, *Chem. Mater.* **2016**, *28*, 2868.
- [56] M. W. Chu, V. Myroshnychenko, C. H. Chen, J. P. Deng, C. Y. Niou, F. J. G. De Abajo, *Nano Lett.* **2009**, *9*, 399.
- [57] P. K. Jain, W. Huang, M. A. El-Sayed, *Nano Lett.* **2007**, *7*, 2080.
- [58] E. Prodan, C. Radloff, N. J. Halas, P. Nordlander, *Science* **2003**, *302*, 419.
- [59] L. Chuntonov, G. Haran, *Nano Lett.* **2011**, *11*, 2440.
- [60] B. Luk'Yanchuk, N. I. Zheludev, S. A. Maier, N. J. Halas, P. Nordlander, H. Giessen, C. T. Chong, *Nat. Mater.* **2010**, *9*, 707.
- [61] C. Krüger, S. Agarwal, A. Greiner, *J. Am. Chem. Soc.* **2008**, *130*, 2710.
- [62] E. M. Go, T. K. Lee, S. H. Min, W. C. Jeon, B. S. Kim, M. S. Yeom, S. K. Kwak, *J. Phys. Chem. C* **2016**, *120*, 11068.
- [63] W. Zhu, R. Esteban, A. G. Borisov, J. J. Baumberg, P. Nordlander, H. J. Lezec, J. Aizpurua, K. B. Crozier, *Nat. Commun.* **2016**, *7*, 11495.
- [64] Y. Cheng, M. Wang, G. Borghs, H. Chen, *Langmuir* **2011**, *27*, 7884.
- [65] R. Kastilani, R. Wong, L. D. Pozzo, *Langmuir* **2018**, *34*, 826.
- [66] G. Marcelo, F. Burns, T. Ribeiro, J. M. G. Martinho, M. P. Tarazona, E. Saiz, M. G. Moffitt, J. P. S. Farinha, *Langmuir* **2017**, *33*, 8201.
- [67] T. Ribeiro, T. J. V. Prazeres, M. Moffitt, J. P. S. Farinha, *J. Phys. Chem. C* **2013**, *117*, 3122.
- [68] R. M. Choueiri, A. Klinkova, H. Thérien-Aubin, M. Rubinstein, E. Kumacheva, *J. Am. Chem. Soc.* **2013**, *135*, 10262.
- [69] C. Yi, H. Liu, S. Zhang, Y. Yang, Y. Zhang, Z. Lu, E. Kumacheva, Z. Nie, *Science* **2020**, *369*, 1369.
- [70] B. Willingham, S. Link, *Opt. Express* **2011**, *19*, 6450.
- [71] C. Hanske, M. Tebbe, C. Kuttner, V. Bieber, V. V. Tsukruk, M. Chanana, T. A. F. König, A. Fery, *Nano Lett.* **2014**, *14*, 6863.

- [72] M. Mayer, P. L. Potapov, D. Pohl, A. M. Steiner, J. Schultz, B. Rellinghaus, A. Lubk, T. A. F. König, A. Fery, *Nano Lett.* **2019**, *19*, 3854.
- [73] F. N. Gür, C. P. T. McPolin, S. Raza, M. Mayer, D. J. Roth, A. M. Steiner, M. Löffler, A. Fery, M. L. Brongersma, A. V. Zayats, T. A. F. König, T. L. Schmidt, *Nano Lett.* **2018**, *18*, 7323.
- [74] M. Yan, *J. Phys. Commun.* **2019**, *3*, 115015.
- [75] P. B. Johnson, R. W. Christy, *Phys. Rev. B* **1972**, *6*, 4370.
- [76] E. M. Roller, L. V. Besteiro, C. Pupp, L. K. Khorashad, A. O. Govorov, T. Liedl, *Nat. Phys.* **2017**, *13*, 761.
- [77] A. F. Stewart, A. Lee, A. Ahmed, S. Ip, E. Kumacheva, G. C. Walker, *ACS Nano* **2014**, *8*, 5462.
- [78] A. Klinkova, H. Therien-Aubin, R. M. Choueiri, M. Rubinstein, E. Kumacheva, *Proc. Natl. Acad. Sci. USA* **2013**, *110*, 18775.
- [79] D. Fava, M. A. Winnik, E. Kumacheva, *Chem. Commun.* **2009**, *18*, 2571.
- [80] R. Liang, J. Xu, W. Li, Y. Liao, K. Wang, J. You, J. Zhu, W. Jiang, *Macromolecules* **2015**, *48*, 256.
- [81] K. Liu, A. Lukach, K. Sugikawa, S. Chung, J. Vickery, H. Therien-Aubin, B. Yang, M. Rubinstein, E. Kumacheva, *Angew. Chem., Int. Ed.* **2014**, *53*, 2648.
- [82] H. Wang, X. Song, C. Liu, J. He, W. H. Chong, H. Chen, *ACS Nano* **2014**, *8*, 8063.
- [83] C. Yi, Y. Yang, Z. Nie, *J. Am. Chem. Soc.* **2019**, *141*, 7917.
- [84] P. Dey, K. J. Thurecht, P. M. Fredericks, I. Blakey, *Macromolecules* **2020**, *53*, 7469.
- [85] C. Rossner, B. Ebeling, P. Vana, *ACS Macro Lett.* **2013**, *2*, 1073.
- [86] C. Rossner, O. Glatter, O. Saldanha, S. Köster, P. Vana, *Langmuir* **2015**, *31*, 10573.
- [87] C. Rossner, B. Ebeling, P. Vana, in *Controlled Radical Polymerization: Materials*, ACS Symposium Series, Vol. 1188, ACS Publications, Washington D.C **2015**, pp. 293–307.
- [88] I. Blakey, Z. Merican, K. J. Thurecht, *Langmuir* **2013**, *29*, 8266.
- [89] P. G. Georgiou, A. N. Baker, S. J. Richards, A. Laezza, M. I. Gibson, M. Walker, M. I. Gibson, *J. Mater. Chem. B* **2019**, *8*, 136.
- [90] C. Fasting, C. A. Schalley, M. Weber, O. Seitz, S. Hecht, B. Kokschi, J. Dervede, C. Graf, E. W. Knapp, R. Haag, *Angew. Chem., Int. Ed.* **2012**, *51*, 10472.
- [91] S. J. Richards, M. I. Gibson, *ACS Macro Lett.* **2014**, *3*, 1004.
- [92] M. Álvarez-Paino, V. Bordegé, R. Cuervo-Rodríguez, A. Muñoz-Bonilla, M. Fernández-García, *Macromol. Chem. Phys.* **2014**, *215*, 1915.
- [93] S. Won, S. J. Richards, M. Walker, M. I. Gibson, *Nanoscale Horiz.* **2017**, *2*, 106.
- [94] S. Won, S. Hindmarsh, M. I. Gibson, *ACS Macro Lett.* **2018**, *7*, 178.
- [95] K. Zhang, X. Zhu, F. Jia, E. Auyeung, C. A. Mirkin, *J. Am. Chem. Soc.* **2013**, *135*, 14102.
- [96] M. Karg, T. A. F. König, M. Retsch, C. Stelling, P. M. Reichstein, T. Honold, M. Thelakkat, A. Fery, *Mater. Today* **2015**, *18*, 185.
- [97] Y. Brasse, M. B. Müller, M. Karg, C. Kuttner, T. A. F. König, A. Fery, *ACS Appl. Mater. Interfaces* **2018**, *10*, 3133.
- [98] R. P. M. Höller, M. Dulle, S. Thomä, M. Mayer, A. M. Steiner, S. Förster, A. Fery, C. Kuttner, M. Chanana, *ACS Nano* **2016**, *10*, 5740.
- [99] P. Dey, S. Zhu, K. J. Thurecht, P. M. Fredericks, I. Blakey, *J. Mater. Chem. B* **2014**, *2*, 2827.
- [100] Y.-C. Chang, L.-C. Huang, S.-Y. Chuang, W.-L. Sun, T.-H. Lin, S.-Y. Chen, *Opt. Express* **2017**, *25*, 24767.
- [101] N. Pazos-Perez, J. M. Fitzgerald, V. Giannini, L. Guerrini, R. A. Alvarez-Puebla, *Nanoscale Adv.* **2019**, *1*, 122.
- [102] C. Kuttner, R. P. M. Höller, M. Quintanilla, M. J. Schnepf, M. Dulle, A. Fery, L. M. Liz-Marzán, *Nanoscale* **2019**, *11*, 17655.
- [103] R. P. M. Ho, C. Kuttner, M. Mayer, R. Wang, M. Dulle, A. Fery, L. M. Liz-Marzán, *ACS Photonics* **2020**, *7*, 1839.
- [104] G. Chen, K. J. Gibson, D. Liu, H. C. Rees, J. H. Lee, W. Xia, R. Lin, H. L. Xin, O. Gang, Y. Weizmann, *Nat. Mater.* **2019**, *18*, 169.
- [105] E. Galati, M. Tebbe, A. Querejeta-Fernández, H. L. Xin, O. Gang, E. B. Zhulina, E. Kumacheva, *ACS Nano* **2017**, *11*, 4995.
- [106] C. Rossner, P. Vana, *Angew. Chem., Int. Ed.* **2014**, *53*, 12639.
- [107] C. Rossner, Q. Tang, O. Glatter, M. Müller, P. Vana, *Langmuir* **2017**, *33*, 2017.
- [108] W. Peng, C. Rossner, V. Roddatis, P. Vana, *ACS Macro Lett.* **2016**, *5*, 1227.
- [109] V. Fedotov, in *Springer Handbook of Electronic and Photonic Materials*, (Eds.: S. Kasap, P. Capper), Springer, Cham **2017**.
- [110] C. M. Soukoulis, S. Linden, M. Wegener, *Science* **2007**, *315*, 47.
- [111] P. Alitalo, S. Tretyakov, *Mater. Today* **2009**, *12*, 22.
- [112] D. Kwon, P. L. Werner, D. H. Werner, *Opt. Express* **2008**, *16*, 9267.
- [113] G. Dolling, C. Enkrich, M. Wegener, J. F. Zhou, C. M. Soukoulis, S. Linden, *Opt. Lett.* **2005**, *30*, 3198.
- [114] S. N. Sheikholeslami, H. Alaeian, A. L. Koh, J. A. Dionne, *Nano Lett.* **2013**, *13*, 4137.
- [115] V. Ponsinet, P. Barois, S. M. Gali, P. Richetti, J. B. Salmon, A. Vallecchi, M. Albani, A. Le Beulze, S. Gomez-Grana, E. Duguet, S. Mornet, M. Treguer-Delapierre, *Phys. Rev. B: Condens. Matter Mater. Phys.* **2015**, *92*, 220414.
- [116] S. K. Ghosh, T. Pal, *Chem. Rev.* **2007**, *107*, 4797.
- [117] C. M. Soukoulis, M. Wegener, *Nat. Photonics* **2011**, *5*, 523.



Christian Roßner is a Liebig fellow and an independent research group leader at the IPF Dresden. He completed his M.Sc. (2013) and PhD (2016) at the University of Göttingen working in the fields of polymer chemistry and nanocomposites with Philipp Vana. He then moved to Graz to focus on electron microscopic characterization of nanomaterials in the group of Gerald Kothleitner (Institute of Electron Microscopy and Nanoanalysis) and subsequently to Toronto to explore surface patterning of nanoparticles together with Eugenia Kumacheva. His research focuses on the design, synthesis, and experimental characterization of polymer-based hybrid nanomaterials for catalytic and sensing applications.



Tobias A. F. König is a Freigeist-Fellow and an independent research group leader at the IPF and Technical University Dresden. He received his diploma from the University of Hamburg (Institute for Laser Physics, 2008) and his Ph.D. from the University of Freiburg (Institute of Microsystems Engineering, 2011). He then worked as a post-doctoral researcher at Georgia Tech, Atlanta, USA (School of Materials Science and Engineering, 2014) and the University of Bayreuth (Institute of Physical Chemistry, 2015). His research focuses on the large-scale self-assembly of colloids and their characterization, using electromagnetic simulation as well as spectroscopic methods for nanophotonic applications.



Andreas Fery is head of the Institute for Physical Chemistry / Polymer Physics at the IPF Dresden and, since 2015, Professor of Physical Chemistry of Polymeric Materials at the Technical University Dresden. After his diploma (University of Konstanz 1996) and Ph.D. (University Potsdam / Max Planck Institute for Colloids and Interfaces, MPIKG, 2000) he worked as post-doctoral researcher at Institute Curie, Paris until 2001 and group leader at MPIKG from 2001-2006. After his habilitation in 2006, he became associate professor and, in 2008, full professor at University Bayreuth. His research focuses on colloids and interfaces, emphasizing colloidal interactions, micro/nano mechanics, pattern formation, and plasmonics.